OPEN EUROPEAN JOURNAL ON VARIABLE STARS
January 2024 http://oejv.physics.muni.cz ISSN 1801-5964
DOI: 10.5817/OEJV2024-0245

CCD PHOTOMETRY, PERIOD ANALYSIS, AND LIGHT CURVE DECONVOLUTION OF THE SHORT PERIOD PULSATING VARIABLE STAR TYC 3603-1124-1

W. ALLEN GILCHRIST, JR.

Stonecrest Observatory, 104 Deer Ridge Drive, Fort Davis, TX 79734, USA gilchrist.allen@ymail.com

Abstract

CCD derived B- and V-magnitudes were determined for Tyc_3603-1124-1, a short period pulsating variable classified as a High Amplitude δ Scuti (HADS) star. Some of these data were acquired during September and October of 2021, and the remainder was recorded in September 2023. Period phased plots of the data showed a slow rise to maximum light but a more rapid drop to minimum brightness. This is somewhat unusual for a HADS star. B-V color indices from 2021 and 2023 were slightly different indicating a possible temperature drop during that period. Additional time-of-maximum data obtained from the SuperWASP extra-solar planet detection program and from the Transiting Exoplanet Survey Satellite (TESS) were combined with Stonecrest Observatory data (SO) in order to perform a predicted time difference (PTD) analysis and obtain an updated linear ephemeris. Fourier analysis of the SuperWASP data yielded only four frequencies with signal-to-noise ratios over SNR=6, but the combined TESS data produced six significantly different frequencies. Regardless of the data source, the first frequencies, F1 ≈ 7.35 and F2 ≈ 14.7 cycles per day, were essentially the same, as was the next frequency, F3 < 0.03 per day. These lower frequencies provided some insight into the noisy appearance of the B and V photometric magnitudes. Stellar parameters for Tyc 3603-1124-1 were not inconsistent with those expected for a HADS variable. Stellar tracks from PARSEC models gave some insight into the evolutionary status of the star.

1. Introduction

The short period pulsating variable star, Tyc 3603-1124-1, is listed in the AAVSO VSX database as a high amplitude δ Scuti (HADS) star, but there are no member contributed (WebObs) observations. VSX lists two references, “The first WASP public data release”, (Butters et al. 2010) and “The All-Sky Automated Survey for Supernovae (ASAS-SN) Light Curve Server v1.0”, (Kochanek et al. 2017). The ASAS-SN site at asas-sn.osu.edu includes a plot of sparsely sampled V-band data from 2014-2015 that clearly shows the variability of this star. There is also a link on the AAVSO VSX site to a phased plot including both the ASAS-SN some CV data that has been adjusted to overlay the V-magnitudes. The web link is:

https://www.aavso.org/vsx_docs/683947/3120/TYC%203603-1124-1%20phase%20curve.png ,

and the plot is included in Figure 1.

DOI: 10.5817/OEJV2024-0245

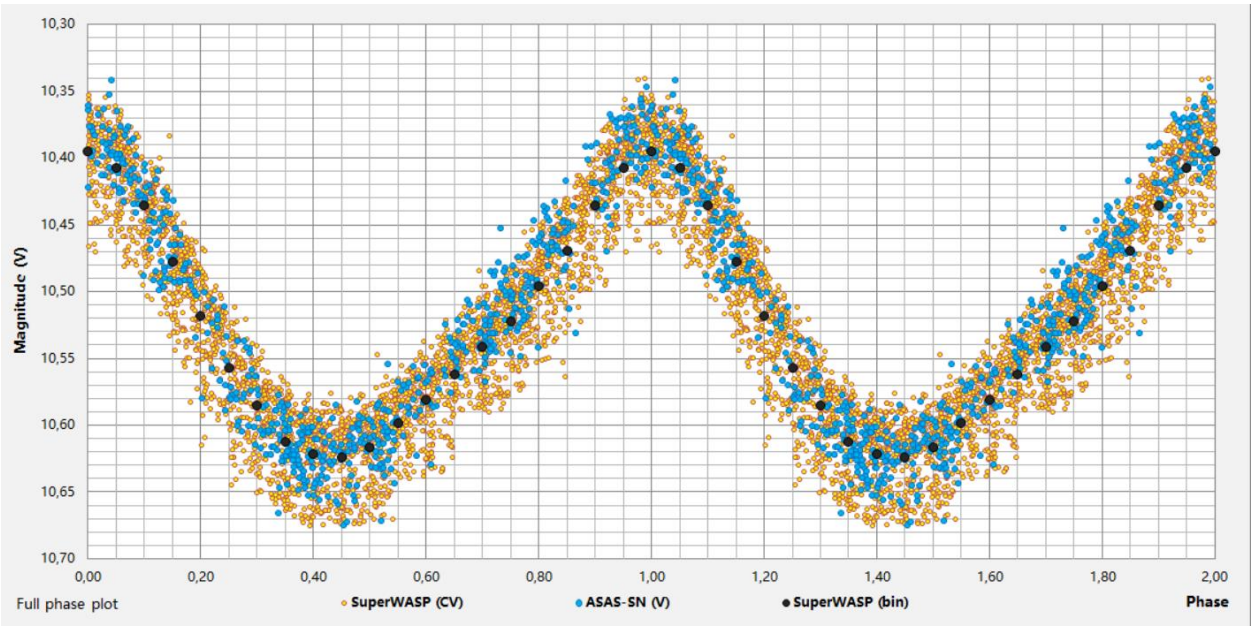

Figure 1. Phased plot of SuperWASP and ASAS-SN data for Tyc 3603-1124-1 from the web site at: https://www.aavso.org/vsx_docs/683947/3120/TYC%203603-1124-1%20phase%20curve.png

A search on the web site at MAST.STSci.edu yielded two large sets of precisely timed high cadence time series flux measurements for Tyc 3603-1124-1 from the Transiting Exoplanet Survey Satellite (TESS) taken between September 2, and October 29, 2022. Altogether, 23,550 individual measurements are included. These data are provided in two large files with flux in e-/s and time in Barycentric Julian Date (BJD). A phased plot of the September data from TESS is included in Figure 2. The phase and scaling were chosen for easy comparison with the SuperWASP values in Figure 1.

January 2024 http://oejv.physics.muni.cz ISSN 1801-5964
DOI: 10.5817/OEJV2024-0245

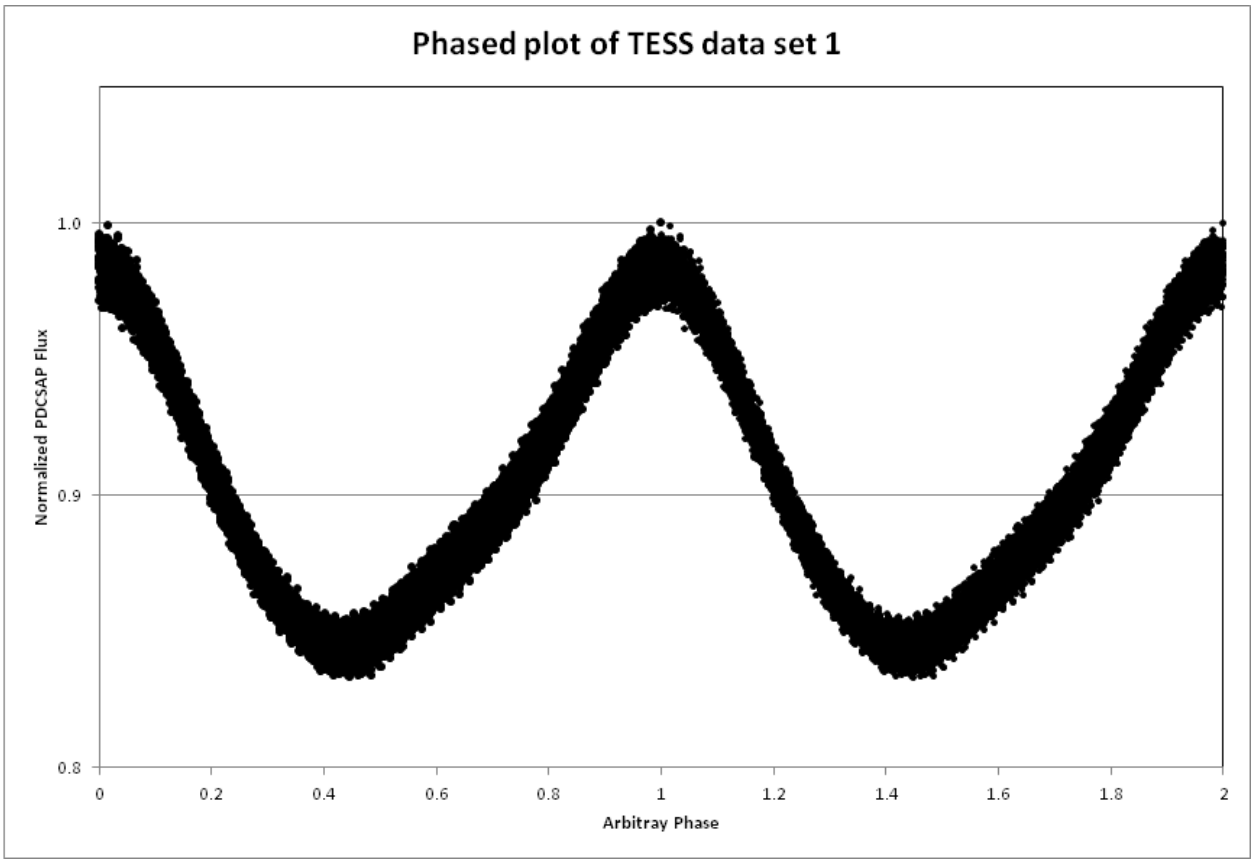

Figure 2. Phased plot of the September, 2022 data from TESS. Note that the values are in normalized flux. The phase and scale were arbitrarily chosen for easy comparison with the SuperWASP data.

Use of all these data will be discussed more fully in the sections on period analysis and Fourier deconvolution.

2. Observations, image reduction, photometric processing, and phased LC plots

2.1 Observations

Precisely timed photometric observations were made from the Stonecrest Observatory (SO) near Fort Davis, TX (103.9767 W. 30.6167 N) with an SBIG ST10-XME CCD camera and SBIG CFW-10 filter wheel mounted at the secondary focus of a 0.3-m f/8 Ritchey Chretien telescope. The system produces a field of view (FOV) of 21x14 arcminutes with an image scale of 1.14 arcseconds/pixel (binned 2x2). SO data for this study were taken during September and October, 2021 and then during August and September, 2023. Image acquisition was done using TheSkyX Pro Version 10.5.0 (Software Bisque 2019) to control the CCD camera, filter wheel, focuser, and an Astro-Physics AP-1200 German equatorial mount. The filter wheel included B and V filters matching the Johnson-Cousins Bessell specification. Exposures of 60 seconds were used for the B filter, with 45 seconds for the V filter.

2.2 Image reduction

Dark subtraction, flat corrections, and image alignment were performed using ImagesPlus Version 6.5 (http://www.mlunsold.com). A few images were registered using AIP4WIN Version 2.4.0 (Berry and Burnell 2005). These programs were also used to compute FWHM or HFD values for use in aperture photometry.

2.3 Photometric processing

Instrumental readings were reduced to catalog-based magnitudes using the APASS star fields (Henden et al. 2009, 2010, 2011; Smith et al. 2011) that are built into MPO Canopus v10.8.5.0 (Minor Planet Observer 2010). Light curves (LCs) were generated using an ensemble of five non-varying comparison stars. The identities, J2000 coordinates, APASS V magnitudes, and color indices (B-V) for Tyc 3603-1124-1 and the comparison stars are provided in Table 1; a corresponding image showing the target and comparison stars is presented in Figure 3.

Table 1. Astrometric coordinates (J2000), V-mag and color indices (B-V) for Tyc 3603-1124-1 and five comparison stars (1-5) used during this study.

ID	RA (2000) h m s	Dec (2000) ° " '	APASS[a] V-mag	APASS[a] B-V
Tyc 3603-1124-1	21 36 25.72	50 38 20.0	10.383	0.365
GSC 3603-1316	21 36 38.11	50 41 40.7	10.918	0.368
GSC 3599-0117	21 35 39.08	50 36 52.5	10.475	0.132
GSC 3599-0742	21 35 57.13	50 34 51.1	10.851	0.301
GSC 3599-1568	21 36 42.31	50 33 20.2	11.628	0.367
GSC 3599-0533	21 36 50.11	50 33 16.1	10.385	0.159

[a]V-mag and (B-V) for comparison stars derived from APASS database described by (Henden et al. 2009, 2010, 2011 and Smith et al. 2011), as well as on the AAVSO web site (http//www:aavso:org/apass)

DOI: 10.5817/OEJV2024-0245

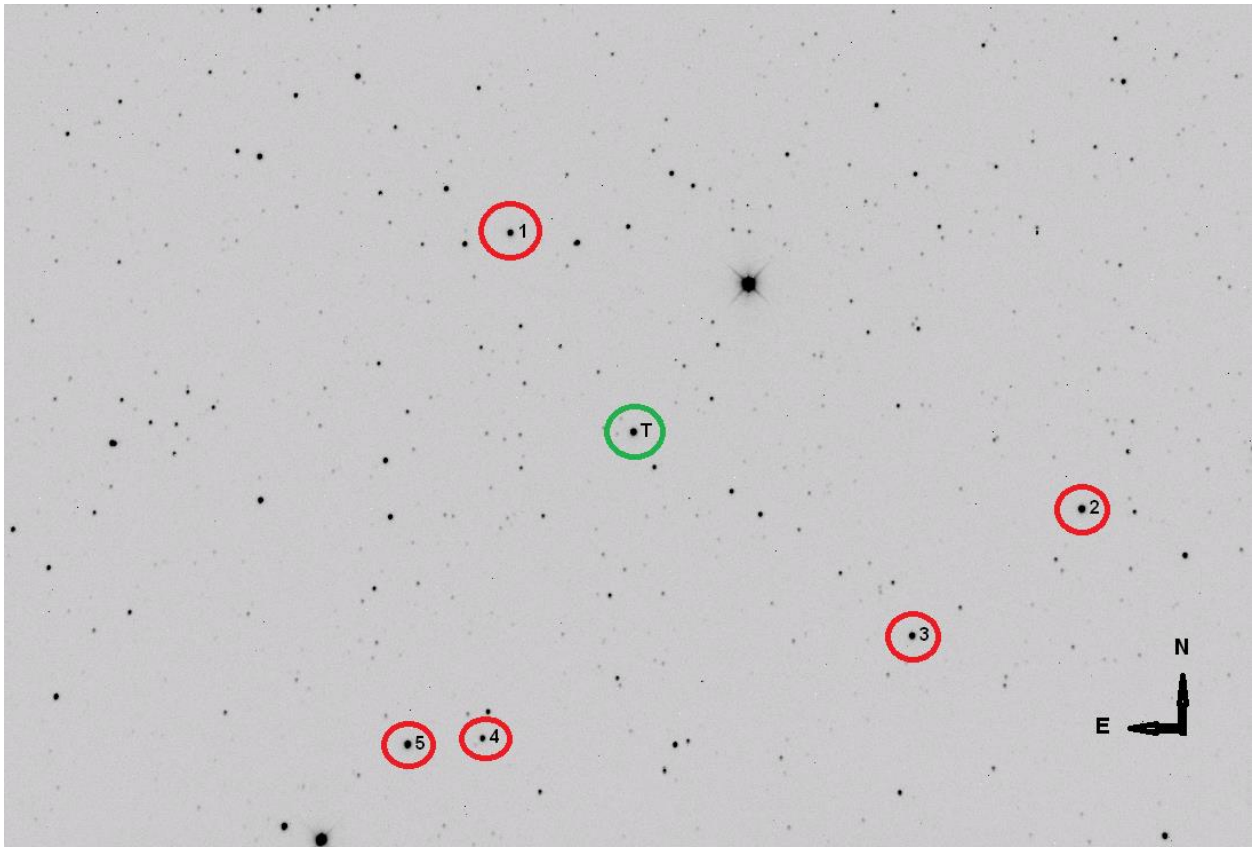

Figure 3. Tyc 3603-1124-1 (green circle) and five comp. stars (red circles) used to reduce time-series images to APASS-catalog based magnitudes.

Only data from images taken above 30° altitude (airmass<2) were included; considering the proximity of all program stars, differential atmospheric extinction was ignored. The average uncertainty in the target star magnitudes for both filters was 0.002 mag. All photometric data acquired and used in this study can be retrieved from the AAVSO international Database (Kafka 2021; observer code GWAA).

There is a remark included in the VSX listing for Tyc 3603-1124-1 stating that the:

> ASAS-SN and SuperWASP magnitudes were contaminated by Gaia DR2 2171362296077209344 (V= 13.0 mag, sep. 1"), also SuperWASP magnitudes contaminated by GSC 03603-00851 (V= 12.4 mag, sep. 40").

Careful examination of a Digitized Sky Survey 2 (DSS2) image of the field in the Aladin Sky Atlas program (V11.0) revealed no stars as bright as m_V = 13.8 closer to Tyc 3603-1124-1 than 27“. The apertures selected for photometric processing easily excluded both the stars mentioned in the VSX remark, and contamination should not be a problem with the B- and V-filter measurements presented in this study. Analysis of SuperWasp and TESS data was limited to Times of maxima, ToMx, and these times should not bt affected by contamination.

3. Results and discussion

DOI: 10.5817/OEJV2024-0245

3.1 Phased LC plots

In order to create phased plots of the SO B and V magnitudes and the B-V color indices, it was necessary to know the period of oscillation. The AAVSO VSX site lists the period as P = 0.1359599 days, and this value was used to produce the phased plots shown in Figure 4.

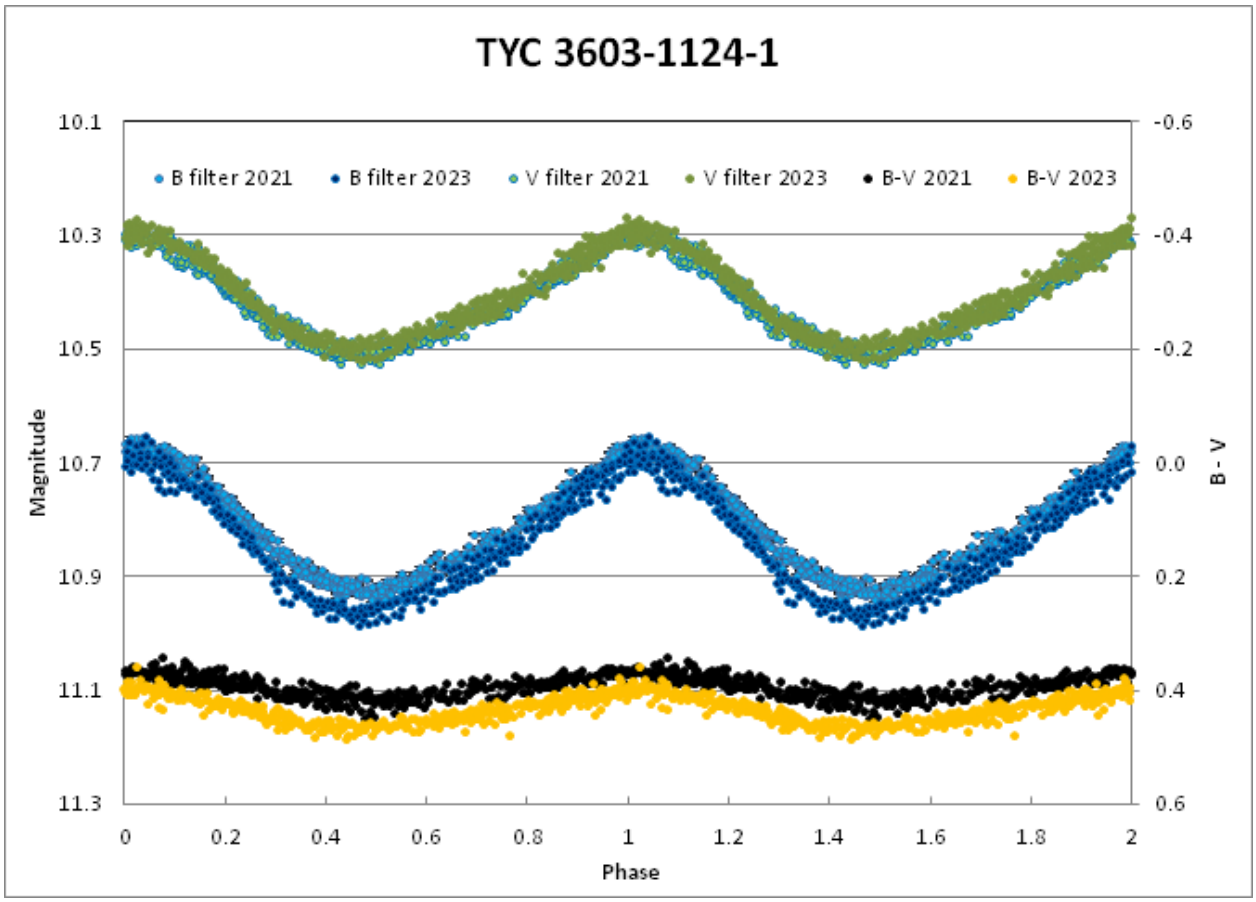

Figure 4. Phased plot of V and B magnitudes and B-V color index for Tyc 3603-1124-1. From top to bottom, the 2023 V-filter magnitudes are in dark green, the 2021 V magnitudes are in light green, The 2021 B-filter magnitudes are in light blue, the 2023 B-filter magnitudes are in dark blue, the 2021 B-V color index values are in black and the 2023 B-V values are in yellow. The phases in this plot were arbitrarily chosen to put the bright portion near phase = 0. The 2021 and 2023 data were phased separately, and there was a small difference of 0.04 with the 2023 points shifted slightly lower (to the left). Close examination reveals that the 2021 V-filter magnitudes are slightly brighter than the 2023 data. The difference in the average values is about -0.02 mag. There is also a difference in the B-filter points, but in this case, the 2023 magnitudes are about 0.016 mags fainter. The overall result is seen in the B-V portion of the plot. The 2023 color index is higher (lower on the plot) indicating a possible reddening of the star during this two year interval.

Near the top of the plot are the V-filter magnitudes with the 2021 points in light green and the 2023 values in dark green. Below that, the B-filter data are presented with the 2021 magnitudes in light blue and the 2023 values in dark blue. The B-V color indices are presented near the bottom of the plot with the 2021 points in black and the 2023 data in yellow. Scales were chosen to keep all the curves separated for clarity. The phases for the 2021 and 2023 data were arbitrarily chosen to place the brightest part of the light curves near

DOI: 10.5817/OEJV2024-0245

phase = 0. There was a slight phase difference of 0.04 between the two data sets with the 2023 values having to be shifted slightly to the left. Error bars are not plotted on this figure, but the uncertainties are approximately the size of the symbols used in the plot.

Averaged over the entire phased LCs, the 2023 V-filter magnitudes are 0.02 brighter than the 2021 data using the same instrument and comparison stars. Considering that these averages are for a star that is varying in brightness, taking the standard deviations of the values over the entire phased LCs would yield an erroneously large uncertainty. A better estimate of the uncertainties in these LCs is the standard deviation of a selected group of points near the maximum or minimum brightness where the values are not rapidly changing. For this study, groups of points near minimum light were used. The uncertainties in the average values will not be larger than these standard deviations. The average V magnitude for the 2021 measurements is $m_V = 10.417 \pm 0.012$, and for 2023 $m_V = 10.397 \pm 0.018$. Similarly, in 2021 $m_B = 10.812 \pm 0.014$ mag., and in 2023 $m_B = 10.822 \pm 0.020$ mag. Since the B-V color indices are more nearly constant, the uncertainties were based on all the measurements. The difference in the B-V color indices from 2021 to 2023 is 0.039 ± 0.031, with the star appearing to have slightly reddened during that time interval. These results could be statistically significant, or they actually might not be. These differences could be the result of low frequency modes altering the mean value and amplitude of the fundamental oscillation. This will be discussed more fully in the section on discrete Fourier transformation (DFT).

The APASS, UCAC4, and 2MASS databases provided additional color information. The first two of these included B and V magnitudes, but the 2MASS catalog only includes j, h and k magnitudes. These can be converted to B and V values using equations listed in the web site at http://brucegary.net/dummies/method0.html. Table 2 includes B-V values from several sources along with uncertainties. Also listed are $(B\text{-}V)_0$ values corrected for interstellar extinction (Amôres and Lépine 2005) along with effective temperatures, T_{eff} (Pecaut and Mamajek 2013). Galactic reddening or color excess, E(B-V), can be found from A_V, equation 1:

$$E(B\text{-}V) = A_V / 3.1 \quad . \qquad (1)$$

E(B-V) can then be used to correct B-V to the intrinsic color, $(B\text{-}V)_0$, using equation 2.

$$(B\text{-}V)_0 = (B\text{-}V) - E(B\text{-}V) \quad . \qquad (2)$$

Estimates for values for the intrinsic color can vary depending on the model selected (Amôres and Lépine 2005, 2007; Schlegel et al. 1998; Schlafly and Finkbeiner 2011; Schlafly et al. 2014). Different models can be accessed via the GALextin website at http://www.galextin.org/ (Amôres et al. 2021). A reddening value of 0.464, based on Amôres and Lépine 2005 was used for this study.

DOI: 10.5817/OEJV2024-0245

Table 2. (B-V), $(B-V)_0$[a], and T_{eff}[b] values for Tyc 3603-1124-1 from SO and other sources.

Source	(B-V)	(B-V) unc	$(B-V)_0$	$(B-V)_0$ unc	log T_{eff}	log T_{eff} unc	T_{eff}	T_{eff} unc
SO (2021)	0.394	0.020	0.244	0.020	3.868	0.003	7550	120
SO(2023)	0.433	0.024	0.283	0.024	3.864	0.004	7300	150
APASS	0.365	0.167	0.215	0.167	3.888	0.056	7722	1000
2MASS	0.899	0.220	0.749	0.220	3.736	0.049	5446	610
UCAC4	0.351	N/A	0.201	N/A	3.843	N/A	6959	N/A

[a]$(B-V)_0$ = (B-V) – E(B-V) where E(B-V) = 0.150 (Amôres and Lépine 2005)
[b]T_{eff} = effective temperature (K) (Pecaut and Mamajek 2013)

The SO temperatures agree within the uncertainties with the value given in the APASS database, and although there is no stated uncertainty for the UCAC4 data, the numbers are still fairly close. The 2MASS temperature estimate is significantly lower, and is considered to be an outlier. An average temperature from the SO data, T_{eff} = 7425 ± 192 K, corresponding to a spectral class of A9V.

Also of interest is the general shape of the LCs. HADS variables usually have asymmetric LCs with a relatively rapid rise from minimum to maximum light and a slower fall from maximum back to minimum (McNamara 2000, Alton and Gilchrist 2021. Alton 2022). Tyc 3603-1124-1 appears to be an exception which is seen in plots of all three data sets (Figures 1, 2, and 4). Rather than a continuous rapid increase to maximum light, the light curve begins with a gentle upward slope before more rapidly increasing to maximum brightness. This unusual rise is followed by an even more rapid drop to minimum brightness.

3.2 Period analysis

The fundamental period of a pulsating variable star, such as Tyc 3603-1124-1 can be assessed in several ways. A starting point is the value of P = 0.1359599 days listed for this star in the AAVSO VSX web page. The lightcurve analysis page in the MPO Canopus program, used for photometric processing of the SO measurements, presents a period, P = 0.1359604 ± 0.0000001 days on a phased plot of magnitudes from several observing runs. **T**he Peranso program (Paunzen and Vanmunster 2016) will determine a period from a set of measurements, and it is quite flexible in handling data from various sources or in different units. A period of P = 0.135931 days was found for each of the three sets of data (SuperWASP, TESS, and SO) for Tyc 3603-1124-1.

Another way of investigating the time series LCs is predicted pulsation time difference (PTD) analysis. This process uses only the measured times of extrema from high cadence time-series measurements, in this case times of maximum brightness (ToMx). These are compared to times predicted by an assumed ephemeris in an iterative process. In this way, an accurate fundamental period of oscillation and an updated ephemeris can be determined. It is also possible to gain insight into any secular changes over the time interval covered by the data. Another advantage of PTD analysis is that data from different sources expressed in different units can be combined. In this case, for Tyc 3603-2411-1, the SuperWASP data are in CV magnitudes, the SO measurements are in B and V magnitudes, and the TESS values are in flux (e-/s). Since only the ToMx times are used, these can all be considered together.

The Peranso program can also be used to determine times of extrema. The program uses periodic orthogonals (Schwarzenberg-Czerny 1996) to fit observations and analysis of variance (ANOVA) to determine fit quality. ToMx values and uncertainties were determined for the SuperWASP, SO, and two sets of TESS data. It is necessary to express all the times on the same scale. The TESS data tables contain times in Barycentric Julian Date – Barycentric Dynamical Time (BJD-TDB), and the SuperWASP and SO values were in Heliocentric Julian Date (HJD). There can be up to a ± 4 s difference between times expressed on the different scales. Fortunately, the Ohio State University maintains a web site at (https://astroutils.astronomy.osu.edu/time/hjd2bjd.html) that can be used to convert times in HJD to BJD_TDB (Eastman, J., et al. 2010). The CV SuperWASP data yielded 66 ToMx values, the TESS results provided 383, and the SO B- and V-filter measurements produced 19.

The VSX reference epoch (February 28, 2014) and the period P = 0.1359599 days combine to define a linear ephemeris (Equation 3):

$$Max\ (HJD) = 2456716.944 + 0.1359599\ E\ . \qquad (3)$$

This period was used as an initial guess in the PTD analysis with subsequent adjustments to determine a new ephemeris that best represented all the data. The resulting new linear ephemeris with uncertainties (Equation 4) is:

$$Max\ (BJD) = (2460191.79078 \pm 0.00007) + (0.135959486 \pm 0.000000005)\ E\ . \qquad (4)$$

Note that the times in equation 4 are in BJD while they are in HJD in equation 3. As stated earlier, there can be up to a ± 4 s difference between times expressed on these two scales, but with all data expressed in BJD, the epoch and period in equation 4 are fine.

Table 3 is a partial list of the ToMx and corresponding PTD (also known as observed minus calculated or O-C) values used in the secular analysis. The table includes only a few of the SuperWASP and TESS measurements, but all of the SO data are incorporated. All times are expressed in BJD. A complete version of Table 3 in a separate file is available online at **https://oejv.physics.muni.cz/issues/data_0245.txt**. During the process of determining ToMx values from the TESS data, it was obvious that the amplitude of the variation and the average brightness of Tyc 3603-1124-1 are not constant. This will be reviewed more fully in the section on Fourier analysis.

Figure 5 shows the resulting fit of the PTD analysis. The SuperWasp data are plotted at the left, the TESS data are in the large block of points toward the right, and the Stonecrest Observatory measurements are the two smaller groups toward the right. The goal was to determine the ephemeris that produces the best (ideally, zero slope and intercept) fit to the data. Linear (red) and quadratic (black) trend lines and the associated equations are included on the plot. By sheer numbers, the SuperWASP and TESS data dominate the linear fit. The negative coefficient for the quadratic term in the parabolic fit would suggest a small (-0.011 sec per year) decrease in the period over the last sixteen years. However the lack of any values between 2008 and 2021 leaves some doubt in the veracity of this solution. In the author's opinion, the variation in the amplitude and mean of the oscillations seen in the TESS data could easily explain these observations. Again, this will be discussed in the section on

January 2024 http://oejv.physics.muni.cz ISSN 1801-5964
DOI: 10.5817/OEJV2024-0245

Fourier analysis. Overall, the results suggest that no significant change in period has occurred since 2007.

DOI: 10.5817/OEJV2024-0245

Table 3. Partial list of ToMx values used in the PTD analysis for Tyc 3603-1124-1.

Source	Bandpass	ToMx BJD[b]-2400000	ToMx Uncertainty	Cycle number	PTD[a]
SuperWASP	CV	54266.675408	0.003432	-43579	-0.00094
SuperWASP	CV	54267.628453	0.001781	-43572	0.00039
SuperWASP	CV	54272.662183	0.004521	-43535	0.00362
SuperWASP	CV	54274.698661	0.003844	-43520	0.00071
SuperWASP	CV	54275.649705	0.002581	-43513	0.00003
Stonecrest	B	59486.708369	0.002090	-5186	0.00348
Stonecrest	V	59486.709349	0.001446	-5185	0.00448
Stonecrest	V	59486.841329	0.001808	-5184	0.0005
Stonecrest	B	59486.842642	0.001685	-5185	0.00179
Stonecrest	B	59493.774786	0.002258	-5134	0
Stonecrest	V	59493.774862	0.002034	-5133	0.0001
Stonecrest	V	59502.748895	0.001701	-5067	0.00081
Stonecrest	B	59502.749108	0.001475	-5068	0.001
Stonecrest	V	59505.606034	0.001140	-5046	0.0028
TESS	TESS[c]	59825.379538	0.001757	-2694	-0.00041
TESS	TESS	59825.513622	0.001739	-2693	-0.00229
TESS	TESS	59825.652858	0.002117	-2692	0.00099
TESS	TESS	59825.788758	0.001796	-2691	0.00093
TESS	TESS	59881.665566	0.002059	-2280	-0.00161
TESS	TESS	59881.802362	0.002287	-2279	-0.00077
TESS	TESS	59881.942063	0.001854	-2278	0.00297
TESS	TESS	59882.073692	0.001596	-2277	-0.00136
Stonecrest	V	60186.621718	0.001960	-38	-0.00261
Stonecrest	B	60186.624122	0.002053	-38	-0.0002
Stonecrest	V	60188.659401	0.002214	-23	-0.00432
Stonecrest	B	60188.659785	0.002021	-23	-0.00393
Stonecrest	B	60188.792265	0.002158	-22	-0.00741
Stonecrest	V	60188.794796	0.002732	-22	-0.00488
Stonecrest	B	60191.651486	0.001957	-1	-0.00334
Stonecrest	V	60191.653184	0.001875	-1	-0.00164
Stonecrest	B	60191.785090	0.003095	0	-0.00569
Stonecrest	V	60191.788815	0.002682	0	-0.00197

[a] PTD = Time difference between observed fundamental mode pulsation time-of-maximum and that calculated using the reference ephemeris (Equation 4).
[b] Times for SuperWASP and SO were converted to BJD using the OSU web site listed in the text.
[c] Bandpass for TESS detector is between 600 and 1000 nm, centered near Cousins Ic.

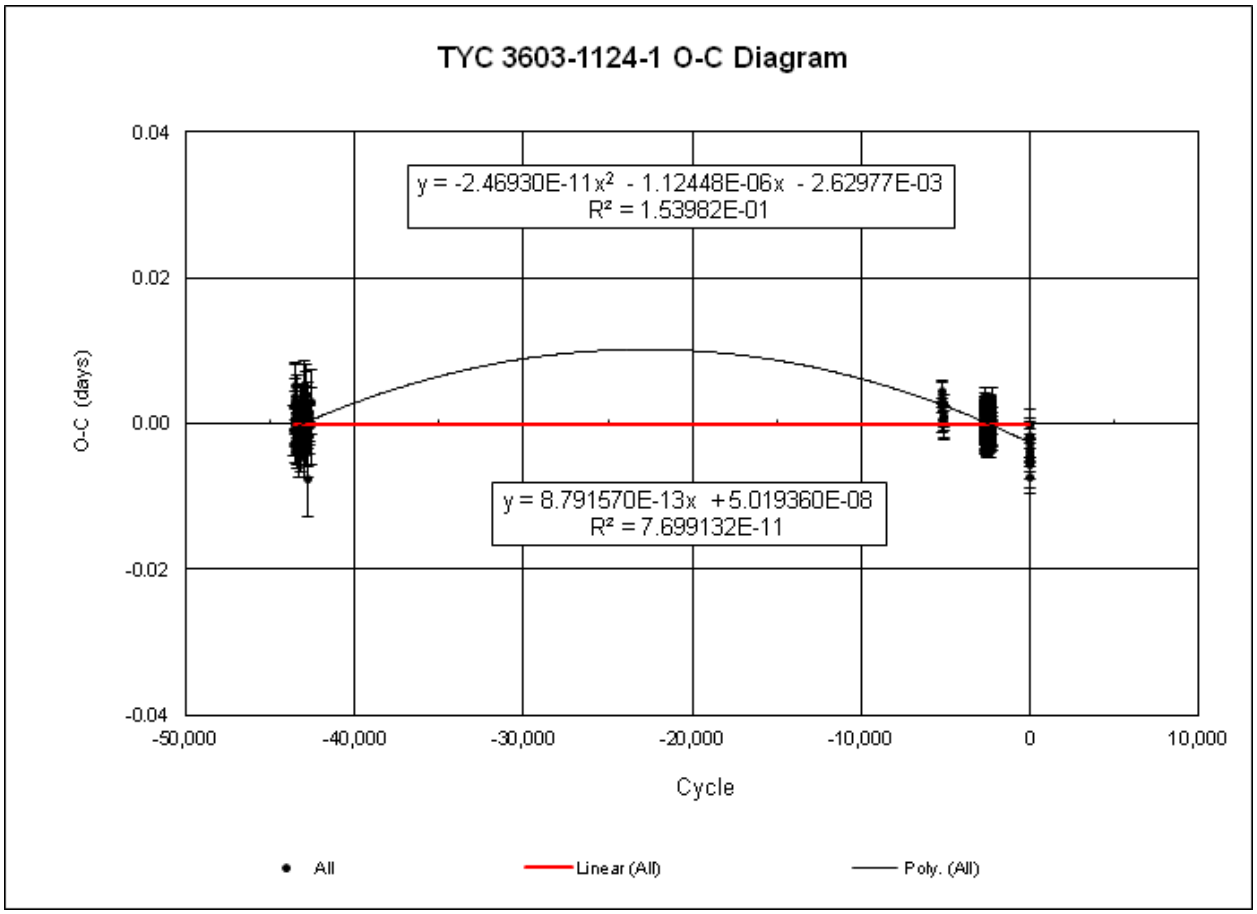

Figure 5. Plot used in the predicted time difference (PTD) analysis. The computed cycle number is plotted on the abscissa and the difference between the observed and computed times of maximum brightness are on the ordinate. The SuperWASP data (taken in Jun. – Oct., 2007) is at the left. The TESS values (taken in Sept. & Oct., 2022) are the large block of data near the right, and the SO points (Sept. & Oct., 2021 and Sept., 2023) are the two smaller groups at the right. The red trend line is the linear fit that resulted in the updated ephemeris in equation 4. These results suggest that no significant change in the period has occurred since 2007.

3.3 Fourier analysis

Period04 (Lenz and Breger 2005) was used to perform discrete Fourier Transformation (DFT) on each group of data. In each case, a fundamental mode pulsating frequency was determined (spectral window = 100 d^{-1}). Subsequent analysis used prewhitening to remove the most significant signals from the previous steps in order to look for oscillations in the residuals. This process was repeated until the signal-to-noise ratio (SNR) fell below six. Analysis of the SuperWASP and SO data both yielded fundamental frequencies near F1 ≈ 7.35 d^{-1}, a harmonic F2 ≈ 14.7 d^{-1}, and a third frequency F3 < 0.034 d^{-1}. Other frequencies had SNR < 6 and were not considered significant. The overwhelming number of measurements (23,550) in the TESS data provided the best basis for DFT analysis. The detection threshold for space-based photometry is significantly higher at S/N ≥ 5.4 than ground-based data at S/N ≥ 4 (Baran et al., 2015 and Baran and Coen, 2021). Frequencies, amplitudes, and phases with uncertainties from the DFT analysis of the TESS data for Tyc 3603-1124-1 are listed in Table

DOI: 10.5817/OEJV2024-0245

4. Uncertainties were determined using the Monte Carlo routine (n=400) built into the Period04 program. The SNR for F7 is less than 6 and that frequency is considered insignificant. Figure 6 shows a spectral window and power spectrum from the DFT in Period04.

Table 4. Frequencies, amplitudes, and phases along with associated uncertainties from DFT analysis of time series photometric TESS data for Tyc 3603-1124-1.

	Freq. d^{-1}	Freq. Unc.[a]	Amp. Norm. Flux	Amp. Unc.	Phase	Phase Unc.	SNR
F1	7.35517	0.00001	0.06458	0.00004	0.19461	0.00011	870.0
F2	14.71061	0.00003	0.01135	0.00004	0.43322	0.00066	188.7
F3	0.19260	0.00006	0.00582	0.00005	0.77075	0.00114	14.5
F4	0.04397	0.00036	0.00418	0.00020	0.32200	0.00196	10.1
F5	0.38432	0.00013	0.00327	0.00004	0.23783	0.00170	9.0
F6	22.06547	0.00013	0.00276	0.00004	0.81635	0.00211	54.0
F7	0.05892	0.00079	0.00205	0.00020	0.42298	0.00439	4.9

[a]Uncertainties in frequency, amplitude, and phase were estimated by the Monte Carlo simulation (n-400) routine built into Period04

Obviously, F1 is the fundamental frequency, F2 is the first harmonic, and F6 is the second harmonic. Between F2 and F6, however, are three low frequency modes. These correspond to variations with periods of 5.2, 22.7, and 2.6 days respectively. These low frequency components appear to come from variations in the mean and amplitude of the flux. Figure 7 is a plot from the Period04 program that presents about a week of the TESS data along with the fit from the DFT analysis. The fundamental oscillation convolved with the lower frequency components is clearly seen. Tyc 3603-1124-1 is probably not a simple radial mode pulsating star.

January 2024 http://oejv.physics.muni.cz ISSN 1801-5964
DOI: 10.5817/OEJV2024-0245

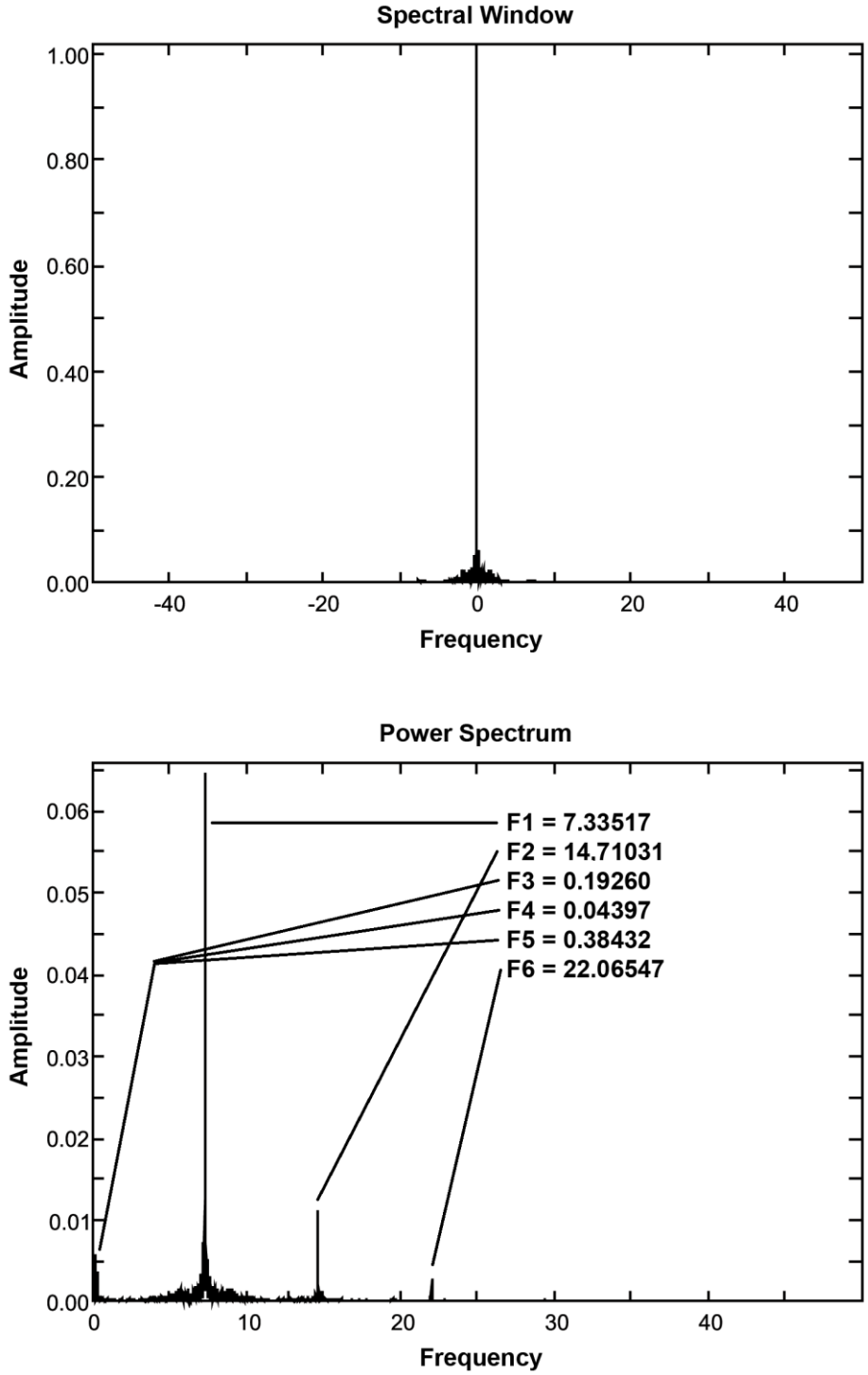

Figure 6. Spectral window and power spectrum plots of the DFT results from the Perios04 program based on the TESS data for Tyc 3603-1124-1. The six statistically significant frequencies are clearly seen in the power spectrum plot. The three low frequency components each have slightly higher amplitudes than the second harmonic, F6.

DOI: 10.5817/OEJV2024-0245

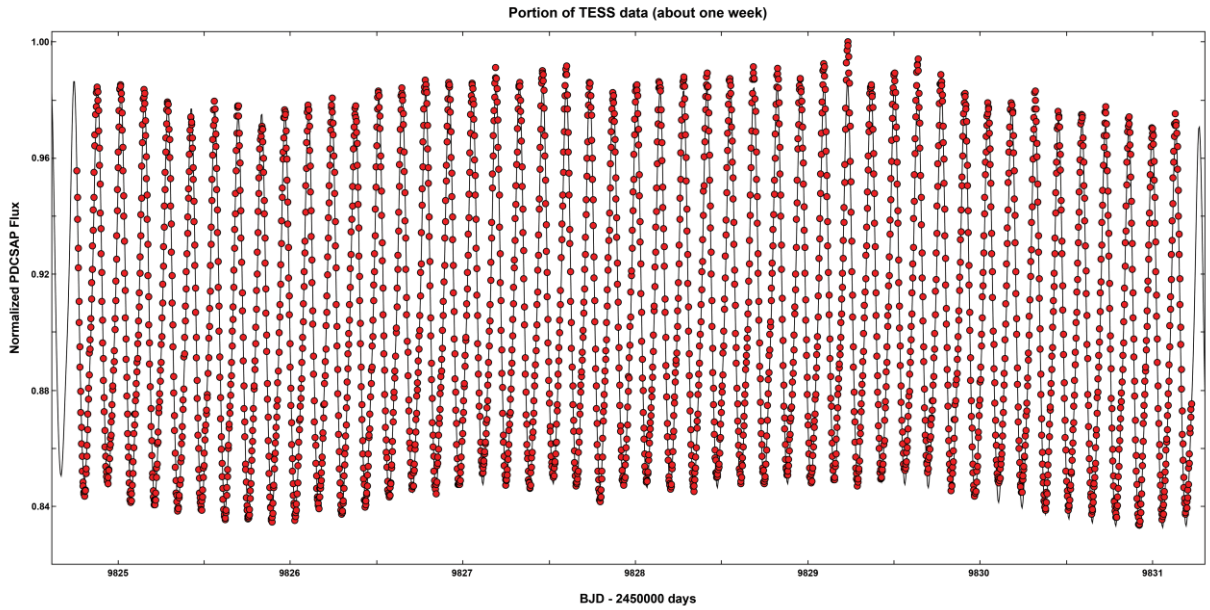

Figure 7. Plot from the Period04 program showing about a week of TESS data for Tyc 3603-1124-1 along with the fit to the data from the DFT analysis. This clearly shows the fundamental period of oscillation convolved with the lower frequency components.

3.4 Stellar parameters

The GAIA DR3 database lists the distance to Tyc 3603-1124-1 as 768 pc and a parallax of 1.3011 ± 0.0142 mas. The uncertainty in the parallax translates into an uncertainty in the distance of ± 8.4 pc. From the SO photometry, the average V magnitude, m_V = 10.417 ± 0.02 mag., and the extinction reddening, A_V = 0.464 mag. These can be combined in the distance modulus (equation 5) to determine the absolute magnitude.

$$M_V = 5 - 5 \log(d) + (m_V - A_V) = 0.529 \pm 0.024 \text{ mag.} \quad (5)$$

The bolometric correction BC_V = 0 for stars in this temperature range (Pecaut and Mamajek 2013). Accordingly, with a solar bolometric magnitude of $M_{bol\odot}$ = 4.75, the luminosity of Tyc 3603-1124-1 in solar units can be calculated using equation 6.

$$L_* = L_\odot \, 10^{\left(\frac{M_{bol\odot} - M_{bol*}}{2.5}\right)} = (48.4 \pm 1.1)\, L_\odot \quad (6)$$

Using this luminosity, along with an average T_{eff} = 7425 ± 192 K and a solar temperature $T_\odot$ = 5772 K, the radius of Tyc 3603-1124-1 can be estimated using equation 7.

$$R_* = R_\odot \sqrt{\frac{L_*}{L_\odot}\left(\frac{T_\odot}{T_*}\right)^4} = (4.2 \pm 0.22)\, R_\odot \quad (7)$$

Eker et al. 2018 present mass-luminosity relationships for main sequence stars in various mass ranges. For stars between 2.4 and 7.0 $M_\odot$, the expression (equation 8) can be used to compute the stellar mass.

$$M_* = M_\odot \cdot 10^{\left(\frac{\log L_* - (0.093 \pm 0.08)}{(3.967 \pm 0.148)}\right)} = (2.52 \pm 0.15) M_\odot \quad (8)$$

DOI: 10.5817/OEJV2024-0245

There is an empirical period-radius relationship for HADS stars presented in Laney et al. 2003. Equation 9 is the expression and with P = 0.135959486 d, the resulting radius provides an independent estimate of R_*.

$$R_* = 10^{((1.106\pm0.012)+(0.725\pm0.01)\cdot\log P+(0.029\pm0.024))} = (3.21 \pm 0.21)\, R_\odot \quad (9)$$

The exponent in equation 9 has two constant terms. The expression represents both HADS and non-HADS pulsating variables. The third term is only used for HADS stars. This radius estimate does not agree within uncertainties with the value from equation 7.

The average density of Tyc 3603-1124-1 can be computed from parameters already calculated. Given a solar mass $m_\odot = (1.98847 \pm 0.00007)\text{x}10^{33}$ g, a solar radius $r_\odot = (6.957 \pm 0.00065)\text{x}10^{10}$ cm, and using the stellar radius, R_*, from equation 7, the stellar density is given by equation 10.

$$\rho_* = \frac{3M_*m_\odot}{4\pi(R_*r_\odot)^3} = (0.0476 \pm .0038)\ g/cm^3 \quad (10)$$

The surface gravity can similarly be determined using equation 11.

$$\log g = log\left(\frac{M_*m_\odot G}{(R_*R_\odot)^2}\right) = (3.827 \pm 0.062)\ cgs \quad (11)$$

The gravitational constant used in equation 11 is $G = 6.67408\cdot10^{-8}$ cm^3 g^{-1} sec^{-2}.

One more parameter of interest for pulsating stars is the pulsation constant (Q). This is the time required for a p-wave to traverse the star. Breger 1990 gives an equation for determining Q if the stellar density, ρ_* is known. Equation 12, with a value of $\rho_\odot = 1.408$ g/cm^3, yields:

$$Q = P\sqrt{\rho_*/\rho_\odot} = (0.025 \pm 0.001)\ d \quad (12)$$

The observations and computed stellar parameters produced in this study are reasonably consistent with those expected for a HADS variable. The fundamental period of pulsation, P = 0.135959486 ± 0.000000005 d, the effective temperature, T_{eff} = 7425 ± 192 K (corresponding to a spectral class of A9), and the computed stellar parameters fit fairly well. There is still the issue of the unusual shape of the LC. Phased LCs, from all sources, exhibit a relatively slow rise from minimum brightness that speeds up slightly as the star approaches maximum brightness. Then the drop from maximum to minimum brightness is even more rapid.

3.5 Evolutionary status of Tyc 3603-1124-1

With estimates for luminosity and the effective temperature for Tyc 3603-1124-1, it is possible to attempt to describe the evolutionary status of this variable. Figure 8 is a plot of a theoretical Hertzsprung-Russell diagram (HRD).

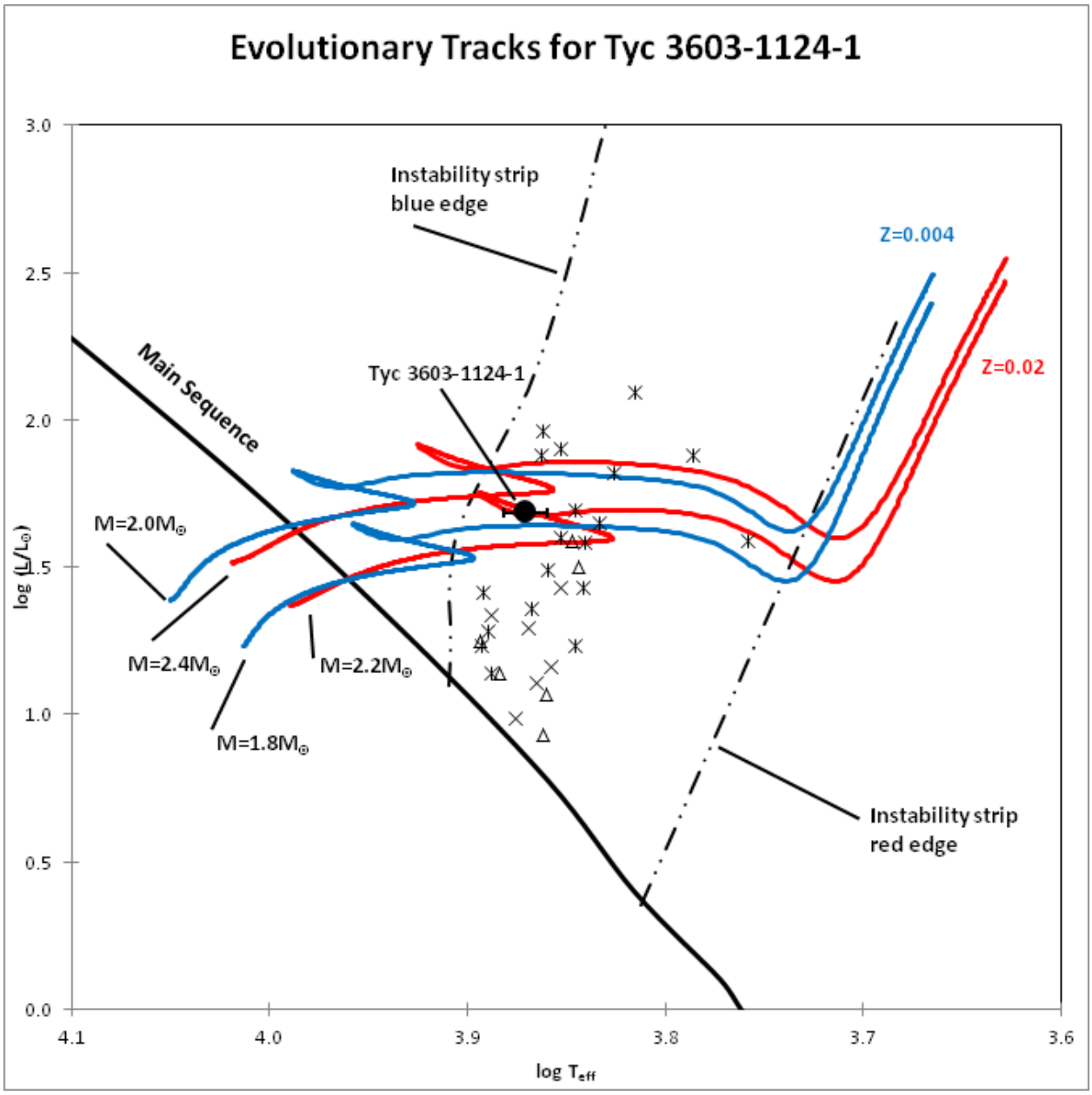

Figure 8. Evolutionary tracks derived from PARSEC models (Bressan *et al.* 2012) are presented as red solid lines for Z = 0.020 at $M_* = 2.2$ and 2.4 $M_\odot$ and blue lines for Z = 0.004 at $M_* = 1.8$ and 2.0 $M_\odot$. The position of Tyc 3603-1124-1 (●) is shown relative to ZAMS (solid black line) and within the theoretical instability strip for radial low-p mode pulsators (dashed lines). Asterisks denote the positions of known HADS stars while open triangles (Δ) indicate the position of SX Phe stars (Balona 2018). X symbols mark the positions of HADS stars from more recent publications (Alton and Kazimierz 2019; Alton 2019; Alton and Gilchrist 2022; Alton 2022; Gilchrist and Alton 2023).

Here, the thick solid line gives the ZAMS position while two broken lines show the blue and red edges of the theoretical instability strip for radial low-p modes (Xiong et al. 2016). The positions of several known HADS stars, including both δ Sct (*) and SX Phe (Δ), (Balona 2018) are plotted as are a few stars (x) from more recent papers (Alton and Kazimierz 2019; Alton 2019; Alton and Gilchrist 2022; Alton 2022; Gilchrist and Alton 2023). The solid filled

circle shows the position of Tyc 3603-1124-1 using the SO derived parameters and corresponding uncertainty estimates (the uncertainty in the luminosity is smaller than the size of the symbol). To estimate the mass and age of a star from theoretical evolutionary tracks the star's metallicity, Z, must be known. Unfortunately, no high resolution spectra are available for Tyc 3603-1124-1 so no direct measurement of Z exists. It is possible; however, try to estimate its value indirectly. With a galactic latitude of 1.122°, Tyc 3603-1124-1 is most likely member of the galactic disc rather than a halo object. It can therefore be assumed that the metallicity is close to that of our Sun, or perhaps a little lower. This is similar to the metallicity of globular cluster stars classified as Oosterhoff type I. Interestingly, the exact value of the metallicity of the Sun remains a point of contention. Numbers obtained in the last few decades range between 0.012 and 0.020. A more complete discussion of solar metallicity is given in Gilchrist and Alton 2023, Four different PARSEC evolutionary models (Bressan et al. 2012) are plotted in Figure 8: the red solid lines show the models when Z= 0.020 and blue solid lines define the models with Z = 0.004. The lower-Z models correspond to a decrease in metallicity by a factor of about 3 to 5 depending on the reference solar metallicity. The plotted position of Tyc 3603-1124-1 falls between the two blue curves presented, but these models are for stellar masses of 1.8 and 2.0 $M_\odot$, much lower than the value of 2.52 ± 0.15 $M_\odot$ calculated in the section on stellar parameters. If we assume, however, that Z=0.020, Figure 8 shows the point for Tyc 3603-1124-1 falling between the red curves for 2.2 and 2.4 $M_\odot$. Both of these are lower than the computed value, but the higher mass model is within the uncertainty in the mass calculated in the section on stellar parameters. The closest approach of the $M_* = 2.2\ M_\odot$ model to the plotted position of Tyc 3603-1124-1 is for a star of $9.47 \cdot 10^8$ years of age with a stellar radius of $R_* = 4.28\ R_\odot$. The point falls along a loop in the evolutionary model that is due to a stellar contraction near the end of hydrogen burning in the core. The closest approach of the $M_* = 2.4\ M_\odot$ model is for a somewhat younger star of $6.68 \cdot 10^8$ years with a radius of $R_* = 3.99\ R_\odot$. Both of these stellar radius values are fairly close the values presented in the section on stellar parameters. Another way to compare the plotted position of the SO temperature and luminosity with the PARSEC models is to interpolate the values between the various model curves. Table 5 lists the resulting stellar parameters along with the values determined from the SO measurements alone. Note that only the Z=0.02 models were used. The uncertainties in the PARSEC derived parameters are based on similar interpolations of the uncertainty envelope of the plotted point from the SO measurements. Obviously, none of the uncertainties are actually zero, but some of them are too small to express in the number of figures presented in the table.

Table 5. Stellar parameters for Tyc 3603-1124-1 using values from observations at SO and those predicted from evolutionary modelling with Z=0.02 (PARSEC[a]).

Parameter	PARSEC[b]	PARSEC[c]	SO
Mean Teff (K)	7425±192	7418±50	7425±192
Mass ($M_\odot$)	2.33±0.005	2.2±0.00	2.52±0.15
Radius ($R_\odot$)	4.21±0.22	4.22±0.07	4.2±0.22
Luminosity ($L_\odot$)	48.4±0.008	48.4±0.23	48.4±1.1
Age (Gyr)	0.756±0.022	0.947±0.00	--

[a] Bressan et al., 2012

[b] Interpolation between Z=Mass=2.2 and 2.4 $M_\odot$

[c] Interpolation of values on the loop in the 2.2 $M_\odot$ model

DOI: 10.5817/OEJV2024-0245

Two sets of parameters are included, one from an interpolation between the Mass = 2.2 $M_\odot$ and the Mass = 2.4 $M_\odot$ models, and the other from the loop on the 2.2 $M_\odot$ model. The author prefers the former as it yields a mass closer to the value computed from the SO measurements. These results still leave some question about the evolutional status of Tyc 3603-1124-1. This question might ultimately be answered in the future if high resolution spectroscopic data can be obtained for the star.

4. Conclusions

The light curve from TYC 3603-112-1 has a somewhat unusual shape when compared to other HADS variables historically and more recently reported in the literature. The shapes of the LCs, from all sources, do not have the rapid rise to brightness and slower decline that is usual for HADS stars. Photometric measurements taken by the author at SO contained more scatter than expected, and there was a noticeable difference between results from measurements taken in 2021 and 2023. These are most probably due to the intrinsic variability in the light curve extrema as seen in the TESS data. PTD analysis of 19 ToMx times from the SO measurements along with 66 ToMx times from SuperWASP and 383 ToMx times from TESS data were used to produce a new linear ephemeris. These results suggested that the fundamental period of oscillation has been stable over the last sixteen years. The average temperature, T_{eff} = 7425 ± 192 K, based on the B- and V-band SO measurements, agrees within uncertainties with the value given in the APASS database, and is close to the value in the UCAC4 database. This temperature corresponds to a spectral class of A9V. Fourier analysis showed a fundamental mode with two overtones convolved with three low frequency modes. The low frequency, day-to-day, changes in average brightness and amplitude of the higher frequency oscillations could easily explain the scatter and year-to-year differences seen in the SO measurements. Calculations of various stellar parameters based on SO measurements produced results which are fairly consistent with what might be expected of a HADS star. Comparison of the T_{eff} and luminosity of Tyc3603-1124-1 with stellar evolution tracks from PARSEC models suggest that the star is a HADS variable with near solar metallicity and a mass in the range $2.33 < M_* < 2.5\ M_\odot$.

5. Acknowledgements

The author gratefully acknowledges the help of his AAVSO mentor, Kevin B. Alton, for all his help in getting started in variable star photometry. Important data and references were found in the Variable Star Index (VSX) accessed through the AAVSO web page. The Mikulski Archive for Space Telescopes at MAST.STSci.edu provided easy search and download for the Transiting Exoplanet Survey Satellite (TESS) data. The CDS-VizieR web site provided by the Centre de Donnes astronomiques de Strasbourg, France (https://vizier.cds.unistra.fr/viz-bin/VizieR) provided valuable access to numerous databases including GAIA DR2, GAIA DR3, TESS, and others. Thanks must also go to the Ohio State University for providing conversion from HJD to BJD on their web site at (https://astroutils.astronomy.osu.edu/time/hjd2bjd.html). Finally, the author gratefully acknowledges the careful review and commentary provided by the journal referees and editors.

References

Alton, K.B. and Kazimierz, S., 2019, JAAVSO, **47**, 53. 2019JAVSO..47...53A
Alton, K.B., 2019, JAAVSO, **47**, 231. 2019JAVSO..47..231A
Alton, K.B. and Gilchrist, W.A., 2021, JAAVSO, **50**, 1, 61. 2022JAVSO..50...61A
Alton, K.B., 2022, JAAVSO, **50**, 2, 218. 2022JAVSO..50..218A
Amôres, E.B. and Lépine, J.R.D., 2005, Astron. J., **130**, 650. 2005AJ....130..659A
Amôres, E.B., Jesus, R.M., Moitinho, A. et al., 2021, MNRAS, **508**, 1788. 2021MNRAS.508.1788A
Balona, L. A., 2018, Mon. Not. Roy. Astron. Soc., **479**, 183. 2018MNRAS.479..183B
Baran, A.S., Koen, C., and Porkrzywka, B., 2015, MNRAS, **448**, 116. 2015MNRAS.448L..16B
Baran, A.S., and Koen, C., 2021, Acta Astron., **71**, 113. 2021AcA....71..113B
Bressan, A., Marigo, P., Girardi, L. et al., 2012, MNRAS, **427**, 127. 2012MNRAS.427..127B
Berry, R., and Burnell, J., 2005, *Handbook of Astronomical Image Processing*, Willmann-Bell, Richmond. 2005haip.book.....B
Breger, M., 1990, Delta Scuti Newsl., **2**, 13. 1990DSSN....2...13B
Butters, O.W. et al., 2010, *A&A*, **520**, L10 2010A&A...520L..10B
Eastman, J., Siverd, R., and Gaudi, B.S., 2010, Publ. Astron. Soc. Pacific, **122**, 935. 2010PASP..122..935E
Eker, Z. et al., 2018, Mon. Not. Roy. Astron. Soc., **479**, 5491. 2018MNRAS.479.5491E
Gilchrist, W.A. and Alton, K.B., 2023, JAAVSO, **51**, 211. 2023JAVSO..51..211G
Henden, A.A., Welch, D.L., Terrell, D. and Levine, S.E., 2009, Bull. Amer. Astron. Soc., **41**. 2009AAS...21440702H
Henden, A. A., Terrell, D., Welch, D. and Smith, T. C., 2010, Bull. Amer. Astron. Soc., **42**. 2010AAS...21547011H
Henden, A. A., Levine, S. E., Terrell, D. et al., 2011, Bull. Amer. Astron. Soc., **43**. 2011AAS...21812601H
Kochanek, C.S. et al., 2017, Publ. Astron. Soc. Pacific, **129**, 980. 2017PASP..129j4502K
Lenz, P., and Breger, M., 2005, Commun. Asteroseismology, **146**, 53. 2005CoAst.146...53L
McNamara, D.H., 2000, Astron. Soc. Pacific Conference Series, **210**, 373. 2000ASPC..210..373M
Minor Planet Observer. 2010, MPO Software Suite (http://www.minorplanetobserver.com), BDW Publishing, Colorado Springs.
Paunzen, E. and Vanmunster, T., 2016, Astron. Nachr., **337**, 239. 2016AN....337..239P
Pecaut, M.J. and Mamajek, E.E., 2013, Ap.J.S., **208**, 9 2013ApJS..208....9P
Peña-Garay, C., 2016, Mon. Not. Roy. Astron. Soc., **463**, 2. 2016MNRAS.463....2S
Schlafly, E.F., and Finkbeiner, D.P., 2011, Astrophys. J., **737**, 103. 2011ApJ...737..103S
Schlafly, E.F. et al., 2014, *Astrophys. J.*, **789**, 15. 2014ApJ...789...15S
Schlegel, D. J., Finkbeiner, D. P., and Davis, M., 1998, Astrophys. J., **500**, 525. 1998ApJ...500..525S
Schwarzenberg-Czerny, A., 1996, Astrophys. J., **460**, L107. 1996ApJ...460L.107S
Smith, T.C., Henden, A.A. and Starkey, D.R., 2011, Proceedings of the Soc. Astron. Sci., **30**, 121. 2011SASS...30..121S
Software Bisque 2019, TheSkyX Professional https://www.bisque.com/product/theskyx-pro/